A computational contact model for nanoscale rubber adhesion

Roger A. Sauer
Institute for Continuum Mechanics, Leibniz Universität Hannover, Germany

published in *Constitutive Models for Rubber VI*, G. Heinrich et al. (Eds.), Taylor & Francis, London, pp. 47-52, 2009

ABSTRACT: We present a continuum mechanical contact model which is capable of describing and simulating rubber adhesion at the nanometer scale. The formulation is based on the coarse-graining of the molecular interaction, like van der Waals attraction, between neighboring solids during contact. A nonlinear finite element implementation of the model is presented which allows the efficient simulation of adhesive contact problems at the range between several nanometers and a few micrometers. The model shows excellent agreement with the analytical JKR theory in the range where the JKR model is applicable. The model behavior is illustrated by several numerical examples. As an application of the contact model the nanoindentation of a thin rubber film is considered.

1 INTRODUCTION

This research is motivated by understanding and analyzing the nanoscale interactions between two contacting bodies. At this scale long-range interaction forces, like van der Waals adhesion, play a crucial role in determining the contact behavior. In many cases molecular adhesion carries over to macroscale problems. Examples include gecko adhesion and rubber adhesion on smooth surfaces. The mechanisms furnishing the transition of adhesion from the nanoscale to the macroscale are a topic of active research. Key factors facilitating the transition are the compliance of the bodies and the surface roughness on the intermediate scales.

In (Sauer and Li 2007b) we have proposed a computational model for nanoscale contact, termed the coarse-grained contact model (CGCM), that offers great flexibility in analyzing general contact problems at the range of a few nanometers to many hundreds of nanometers accurately, and which can be used in computational multiscale techniques to be applied at even larger scales (Sauer 2009).

This paper gives an overview of the coarse grained contact model and discusses its application to rubber adhesion. The overview of the theoretical and computational framework of the CGC model is given in sections 2, 3 and 4. For validation, section 5 presents a comparison between the CGC model and the widely used JKR theory. In section 6 the application of the CGC model to the nanoindentation of a thin rubber film is considered. Section 7 concludes this paper.

2 A CONTINUUM ADHESION MODEL

This section provides an overview of the coarse-grained contact model (Sauer and Li 2007b), which is suitable to model nanoscale rubber adhesion. We consider two interacting bodies, $\mathcal{B}_1$ and $\mathcal{B}_2$, and suppose that the system is governed by the potential energy

$$\Pi = \sum_{k=1}^{2} \big[\Pi_{\text{int},k} - \Pi_{\text{ext},k}\big] + \Pi_{\text{c}} \,, \tag{1}$$

where

$$\Pi_{\text{int},k} = \int_{\mathcal{B}_{0k}} W_k(\boldsymbol{F}_k)\, \mathrm{d}V_k \tag{2}$$

denotes the internal energy of body $\mathcal{B}_k$ $(k = 1, 2)$. As an alternative to the integration over the reference configuration $\mathcal{B}_{0k}$, $\Pi_{\text{int},k}$ can also be expressed as an integration over the current configuration $\mathcal{B}_k$. W_k denotes the energy density per reference volume. In general, W_k is a function of the deformation gradient $\boldsymbol{F}_k = \operatorname{grad} \boldsymbol{\varphi}_k$.

Adhesive contact is described by the contact interaction energy

$$\Pi_{\text{c}} = \int_{\mathcal{B}_1} \int_{\mathcal{B}_2} \beta_1 \beta_2\, \phi(r)\, \mathrm{d}v_2\, \mathrm{d}v_1 \,, \tag{3}$$

where $\phi(r)$ denotes the interaction energy between the molecules of body $\mathcal{B}_1$ and $\mathcal{B}_2$. Here we use the Lennard Jones potential

$$\phi(r) := \epsilon\Big(\frac{r_0}{r}\Big)^{12} - 2\epsilon\Big(\frac{r_0}{r}\Big)^{6} , \tag{4}$$

which is suitable to model van der Waals adhesion. The quantities β_1 and β_2 denote the molecular densities of bodies $\mathcal{B}_1$ and $\mathcal{B}_2$. These densities refer to the current configuration. The transformation

$$\beta_{0k} = J_k \beta_k , \quad J_k = \det \boldsymbol{F}_k , \quad k = 1, 2 , \tag{5}$$

provides the molecular densities, denoted β_{01} and β_{02}, in the reference configuration.

$\Pi_{\text{ext},k}$ denotes the external energy applied to body $\mathcal{B}_k$ through imposed body forces and surface tractions. The equilibrium configuration of the two interacting bodies is found from setting the variation $\delta\Pi$ equal to zero for all admissible variations of the deformation $\boldsymbol{\varphi}_k$. The variation of the contact energy (3) yields

$$\delta\Pi_{\text{c}} = \sum_{k=1}^{2} \int_{\mathcal{B}_k} \delta\boldsymbol{\varphi}_k \cdot \beta_k \, \boldsymbol{b}_k \, \mathrm{d}v_k \tag{6}$$

where

$$\begin{aligned} \boldsymbol{b}_1(\boldsymbol{x}_1) &:= -\frac{\partial \Phi_2}{\partial \boldsymbol{x}_1} , \quad \Phi_2(\boldsymbol{x}_1) := \int_{\mathcal{B}_2} \beta_2 \, \phi(r) \, \mathrm{d}v_2 , \\ \boldsymbol{b}_2(\boldsymbol{x}_2) &:= -\frac{\partial \Phi_1}{\partial \boldsymbol{x}_2} , \quad \Phi_1(\boldsymbol{x}_2) := \int_{\mathcal{B}_1} \beta_1 \, \phi(r) \, \mathrm{d}v_1 , \end{aligned} \tag{7}$$

denote the interaction forces acting at $\boldsymbol{x}_k \in \mathcal{B}_k$. As seen, they depend on the integration over the neighboring body. Under certain, realistic approximations (Sauer and Wriggers 2009) these forces can be written as

$$\boldsymbol{b}_k(\boldsymbol{x}_k) = \pi \beta_\ell \epsilon r_0^2 \left[\frac{1}{5}\Big(\frac{r_0}{r_k}\Big)^{10} - \Big(\frac{r_0}{r_k}\Big)^{4} \right] \boldsymbol{n}_{\text{p}} , \tag{8}$$

where r_k denotes the closest distance between point $\boldsymbol{x}_k$ and the surface of the neighboring body $\mathcal{B}_\ell$ ($\ell = 1, 2; \neq k$). Vector $\boldsymbol{n}_{\text{p}}$ denotes the surface normal of $\mathcal{B}_\ell$ at the closest projection point of $\boldsymbol{x}_k$. The material parameters β_ℓ and ϵ can be replaced by Hamaker's constant $A_H = 2\pi^2 \beta_{01} \beta_{02} \epsilon r_0^6$ (Israelachvili 1991). Setting $\delta\Pi = 0$ for all admissible variations $\delta\boldsymbol{\varphi}_k$, we obtain the statement

$$\begin{aligned} &\sum_{k=1}^{2} \Bigg[\int_{\mathcal{B}_k} \text{grad}(\delta\boldsymbol{\varphi}_k) : \boldsymbol{\sigma}_k \, \mathrm{d}v_k - \delta\Pi_{\text{ext},k} \\ &- \int_{\mathcal{B}_k} \delta\boldsymbol{\varphi}_k \cdot \beta_k \, \boldsymbol{b}_k \, \mathrm{d}v_k \Bigg] = 0 , \quad \forall \, \delta\boldsymbol{\varphi}_k , \end{aligned} \tag{9}$$

which is the governing weak form of the considered contact problem. Alternatively eq. (9) can also be written as an integration over the reference configuration $\mathcal{B}_{0k}$. Since the contact forces $\boldsymbol{b}_k$, according to eq. (8), vary rapidly, special care is required for the numerical integration of the last term in eq. (9). To improve the numerical integration, an alternative formulation to eq. (9) has been developed in (Sauer and Li 2007b; Sauer and Li 2007a), which is based on surface tractions. We therefore consider

$$\mathrm{d}v_k = c_\ell(r_k) \, \mathrm{d}r_k \, \cos\alpha_k \, \mathrm{d}a_k , \tag{10}$$

where c_ℓ depends on the surface curvature of the neighboring body $\mathcal{B}_\ell$ (Sauer and Wriggers 2009). For small curvatures $c_\ell \to 1$. With the help of relation (10) we can rewrite statement (9) into

$$\begin{aligned} &\sum_{k=1}^{2} \Bigg[\int_{\mathcal{B}_k} \text{grad}(\delta\boldsymbol{\varphi}_k) : \boldsymbol{\sigma}_k \, \mathrm{d}v_k - \delta\Pi_{\text{ext},k} \\ &- \int_{\partial\mathcal{B}_k} \delta\boldsymbol{\varphi}_k \cdot \boldsymbol{t}_k \, \cos\alpha_k \, \mathrm{d}a_k \Bigg] = 0 , \quad \forall \, \delta\boldsymbol{\varphi}_k , \end{aligned} \tag{11}$$

where $\boldsymbol{t}_k$ denotes the contact surface traction defined by

$$\boldsymbol{t}_k := \int_{r_{\text{s}}}^{r_{\text{c}}} c_\ell(r_k) \, \beta_k \, \boldsymbol{b}_k(r_k) \, \mathrm{d}r_k . \tag{12}$$

Considering β_k constant, the integration of eq. (8) yields

$$\boldsymbol{t}_k = \pi \beta_k \beta_\ell \epsilon r_0^3 \left[\frac{1}{45}\Big(\frac{r_0}{r_k}\Big)^{9} - \frac{1}{3}\Big(\frac{r_0}{r_k}\Big)^{3} \right] \boldsymbol{n}_{\text{p}} . \tag{13}$$

Equation (13), together with eq. (11) provide the basis of the finite element implementation of the CGC model that is discussed in the following section. Further details on the derivation reported above and a careful analysis of the accuracy of this model are presented in (Sauer and Wriggers 2009).

3 NONLINEAR FINITE ELEMENT FORMULATION

This section presents the basic finite element equations of the adhesive contact model governed by weak form (11). The focus here is placed on the treatment of the contact integral (the last term in eq. (11)); the treatment of the internal and external integrals can be found in the nonlinear finite element literature, e.g. (Wriggers 2008).

In order to discretize the contact integral, we consider the usual finite element interpolations for the displacement field $\boldsymbol{u}_k$ and its variation $\delta\boldsymbol{\varphi}_k$. Inside each finite element Γ_e that discretizes the surface of $\mathcal{B}_k$, we have

$$\boldsymbol{u}_k \approx \mathbf{N}_e \mathbf{u}_e , \quad \delta\boldsymbol{\varphi}_k \approx \mathbf{N}_e \mathbf{v}_e \tag{14}$$

with

$$\mathbf{N}_e = \left[N_1 \boldsymbol{I} \,,\; N_2 \boldsymbol{I} \,,\; \ldots \,,\; N_{n_e} \boldsymbol{I} \right] , \qquad (15)$$

where N_I denotes the shape function of node I of element Γ_e. The contact integral over the surface element can thus be written as

$$- \int_{\Gamma_k} \delta\boldsymbol{\varphi}_k \cdot \boldsymbol{t}_k \, \cos\alpha_k \, \mathrm{d}a_k = \mathbf{v}_e^T \mathbf{f}_\mathrm{c}^e \,, \qquad (16)$$

where

$$\mathbf{f}_\mathrm{c}^e := - \int_{\Gamma_e} \mathbf{N}_e^T \, \boldsymbol{t}_k \, \cos\alpha_k \, \mathrm{d}a_k \qquad (17)$$

defines the contact force vector acting on the nodes of element Γ_e. For practical computations it is convenient to transform this expression to an integration over the reference configuration of the element as is discussed in (Sauer and Wriggers 2009). That paper also gives further details on the finite element derivation and presents the contact algorithm and the linearization of vector $\mathbf{f}_\mathrm{c}^e$.

4 MODEL PARAMETERS

To characterize the size effect and the adhesional strength of a considered problem we introduce the parameters

$$\gamma_L = \frac{R_0}{r_0} \,, \qquad \gamma_W = \frac{W_0}{w_0} \,. \qquad (18)$$

R_0 and r_0 are two length scales that characterize the overall problem geometry and the nanoscale equilibrium spacing of the Lennard-Jones potential (4). Parameter γ_L thus characterizes the size of the problem in relation to the atomic scale. W_0 and w_0 denote two energy densities that correspond to the energy stored in the elastic deformation and in the adhesion. They are defined as

$$W_0 = E \,, \qquad w_0 = \frac{A_H}{2\pi^2 r_0^3} \,, \qquad (19)$$

where E denotes Young's modulus and A_H denotes Hamaker's constant. According to the definition of Hamaker's constant we can also write $w_0 = \beta_{01}\beta_{02}\epsilon r_0^3$. Parameter γ_W characterizes the bulk stiffness of the problem in relation to the strength of adhesion. A large value of γ_W corresponds to relatively stiff bodies and weak adhesion, whereas a low value for γ_W corresponds to relatively soft bodies and strong adhesion. Typical values for the molecular equilibrium spacing and Hamaker's constant are $r_0 = 0.4\,\mathrm{nm}$ and $A_H = 10^{-19}\,\mathrm{J}$ (Israelachvili 1991).

5 COMPARISON WITH THE JKR MODEL

As a validation of the coarse-grained contact model, we compare it with the analytical contact model of (Maugis 1992). This model is a generalization of the widely used JKR model (Johnson, Kendall, and Roberts 1971), which is often applied to rubber adhesion. The comparison presented here extends the comparison reported in (Sauer and Li 2007a). That paper also lists the equations of the analytical Maugis model. The Maugis model is based on linear half-space theory and applies to the adhesive normal contact of two spheres, where the contact area is much smaller than the radius of the spheres. Here we consider contact between a sphere of radius $R_0 = 21\,\mathrm{nm}$ with a flat half-space (i.e. radius ∞). Considering $r_0 = 0.4\,\mathrm{nm}$, this corresponds to a size parameter of $\gamma_L = 52.5$. In the Maugis model the strength of adhesion is characterized by the parameter $\lambda \in (0, \infty)$. Increasing λ corresponds to increasing adhesion. In fact the limit $\lambda \to \infty$ reproduces the JKR model as a special case. In the present example the adhesion parameter is chosen as $\lambda = 1.3$. Parameter λ is a model specific parameter that has no explicit correspondence to the physically motivated parameter γ_W. It has been found that the value $\gamma_W = 11.55$ produces a remarkable agreement in the following results.

Figure 1 shows the normal contact force P versus the normal contact approach u for the considered problem. For moderate displacements the agreement

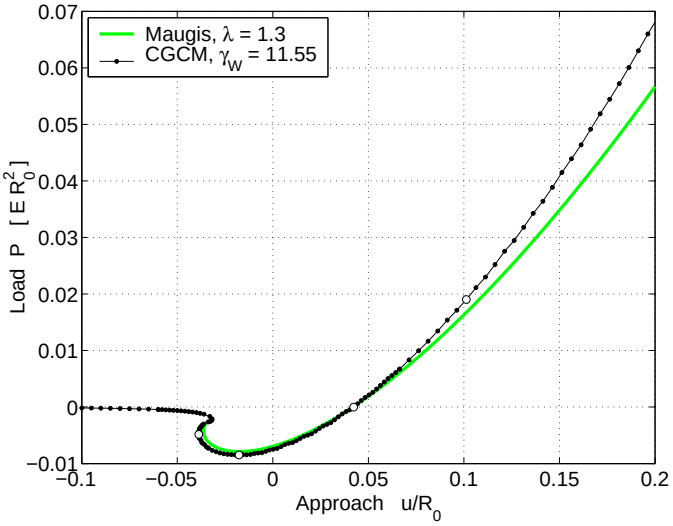

Figure 1: Load displacement curve for a sphere in adhesive contact with a half-space

is excellent. For increasing displacements the two curves diverge since the small deformation assumption used in the Maugis model is no longer valid. For increasing negative displacements, which correspond to separating the bodies, the Maugis model loses its applicability since it is not defined there. For the considered case a contact instability exists, which is in-

dicated by the S-curve in the load-displacement curve (Sauer and Li 2007b).

To further illustrate the agreement between the two models, we examine the radial contact pressure between the two bodies as is shown in figure 2. The pressure distribution according to Maugis and the CGC model is shown in the graphs on the right hand side. The agreement between both models is excellent. The vertical axis displays the radial distance from the symmetry axis measured relative to the sphere radius R_0. The horizontal axis measures the pressure in multiples of Young's modulus E. Altogether, four cases are shown, which correspond to the four states at $u = -0.0388\,R_0$, $u = -0.0176\,R_0$, $u = 0.0423\,R_0$ and $u = 0.1013\,R_0$ that are marked by open circles in figure 1. According to the Maugis model these correspond to $a = 0.050\,R_0$, $a = 0.186\,R_0$, $a = 0.329\,R_0$ and $a = 0.420\,R_0$, where a characterizes the radius of the contact area. The graphs on the left hand side display the deformation of the contact partners together with the stress field σ_z, which is the stress component in the vertical direction. The stress coloring chosen in the figure ranges from $-0.12\,E$ (dark blue) to $0.08\,E$ (dark red). Both the stress field, and the pressure distribution show the smooth repulsive compression at the center of contact and the sharp attractive tension at the contact boundary. The agreement between the two models is much better in the repulsive zone than in attractive zone, which is due to the approximation introduced by Maugis in order to describe the adhesive pressure.

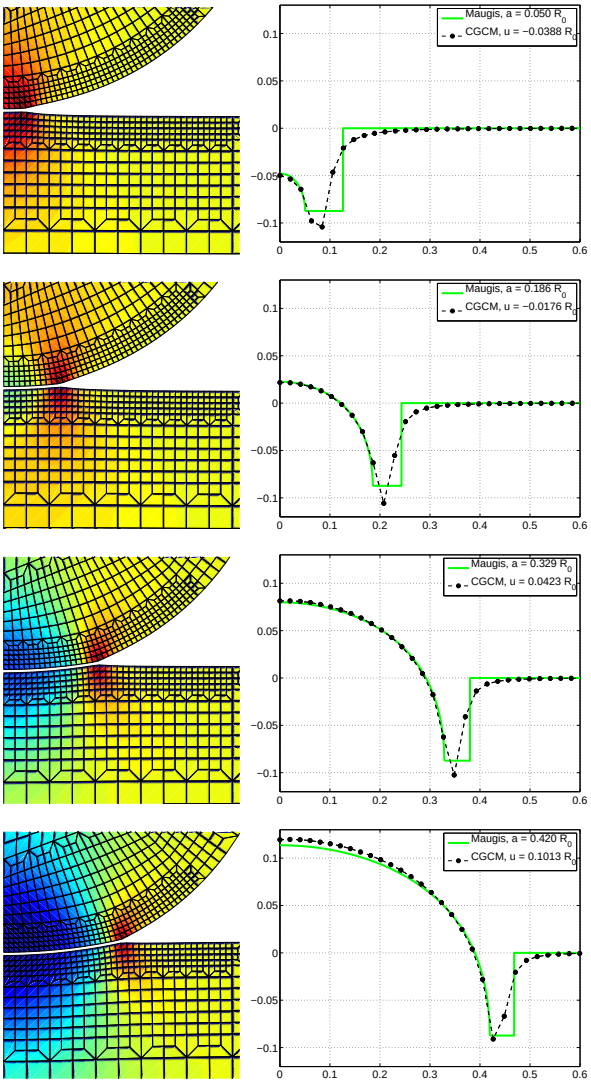

Figure 2: Contact between sphere and half-space: Deformation and stress field (left); contact pressure between the two bodies (right); The four cases correspond to the four states marked in figure 1.

Further comparison examples, along with detailed discussions, are given in (Sauer and Li 2007a).

6 NANOINDENTATION EXAMPLE

As a numerical example of the coarse grained contact model we compute the 3D nanoindentation of a thin rubber film. A rigid Vickers indenter is considered, which is a four-sided pyramidal indenter with an opening angle of $2 \times 68°$ between opposing faces. The indenter is pressed into the thin film which has a considered thickness of $R_0 = 10\,\text{nm}$. Considering $r_0 = 0.4\,\text{nm}$, this corresponds to a size parameter of $\gamma_L = 25$. Initially a gap of $g_0 = 1.5 r_0 = 0.06 R_0$ is chosen between the indenter tip and the film surface. The rubber film is considered perfectly bonded to an underlying rigid substrate. The rubber material is considered nearly incompressible, and is described by the Neo-Hookean material model

$$W(J, \hat{\boldsymbol{C}}) = U(J) + \tfrac{\mu}{2}(\hat{I}_1 - 3)\,, \qquad (20)$$

which is based on a split between the volumetric deformation, described by the determinant of the deformation gradient

$$J = \det \boldsymbol{F}\,, \qquad (21)$$

and the deviatoric deformation, characterized by

$$\hat{I}_1 = \operatorname{tr} \hat{\boldsymbol{C}}\,, \quad \hat{\boldsymbol{C}} = \hat{\boldsymbol{F}}^T \hat{\boldsymbol{F}}\,, \quad \hat{\boldsymbol{F}} = J^{-\frac{1}{3}} \boldsymbol{F}\,. \qquad (22)$$

The volumetric strain energy is taken as

$$U(J) = \tfrac{K}{4}(J^2 - 1) - \tfrac{K}{2} \ln J\,. \qquad (23)$$

Parameters K and μ denote the bulk and shear modulus which are related to Young's modulus E and Poisson's ratio ν according to

$$K = \frac{E}{3(1-2\nu)}\,, \quad \mu = \frac{E}{2(1+\nu)}\,. \qquad (24)$$

In the following example Poisson's ratio is chosen as $\nu = 0.499$. E is used for normalization and can thus be left unspecified.

For the following indentation computations a Q1P0 finite element formulation for large deformations is used (Wriggers 2008). Due to symmetry only a quarter segment of the film is modeled. A segment size of $R_0 \times 3R_0 \times 3R_0$ is chosen.

Figure 3 shows the load displacement curves in the range $u \in (-0.1\,R_0,\, 0.5\,R_0)$ for the cases of weak adhesion ($\gamma_W = 1000$) and strong adhesion ($\gamma_W = 10$). The difference between both cases is revealed by the

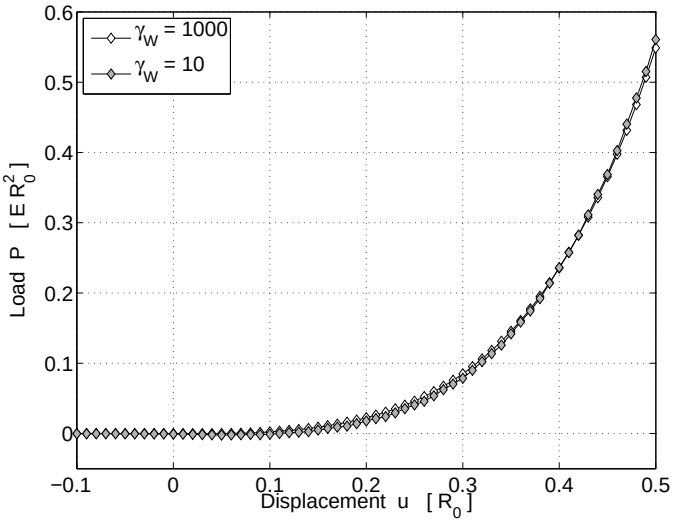

Figure 3: Load displacement curve $P(u)$ for indentation with weak adhesion ($\gamma_W = 1000$) and strong adhesion ($\gamma_W = 10$)

enlargement shown in figure 4. For $\gamma_W = 10$ consid-

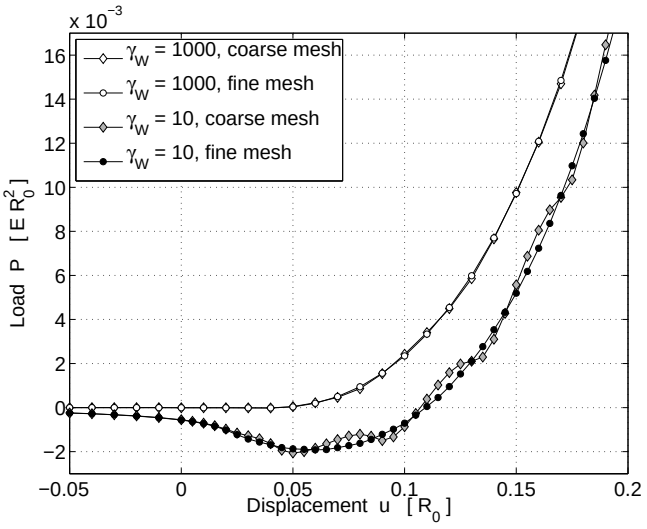

Figure 4: Enlargement of the load displacement curve from figure 3

erable attraction ($P < 0$) exists between the bodies prior to contact. For $\gamma_W = 1000$ the attractive forces between the bodies are negligible and the resultant contact load P is positive. Further, figure 4 shows the results for two different meshes: a coarse mesh with 10 elements along R_0 and a fine mesh with 25 elements along R_0. The figure shows that for $\gamma_W = 1000$ (weak adhesion) the difference between both meshes is very small. For $\gamma_W = 10$ (strong adhesion) however, the coarse mesh causes a large error so that the difference between the coarse and fine mesh is quite large. This shows that for increasing adhesion finer meshes must be used in order to maintain accurate computational results.

Figure 5 and 6 display the deformation at $u = 0.5R_0$ for $\gamma_W = 1000$, where adhesion is negligible, and $\gamma_W = 2.17$, where the adhesion is very strong. As can be seen, strong adhesion leads to large tensile

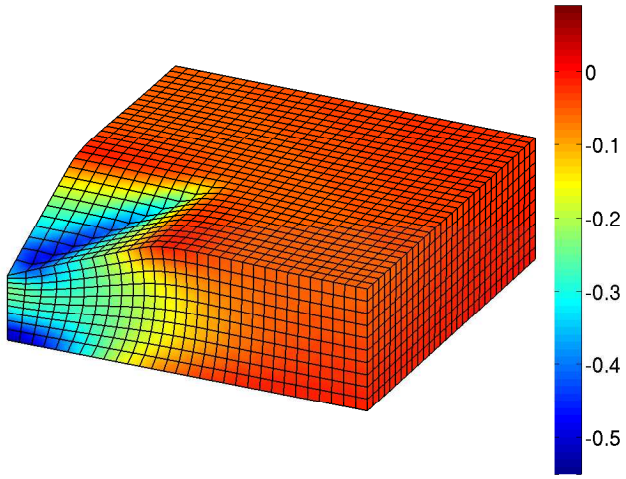

Figure 5: Nanoindentation of a rubber film: deformation and stress field under the indenter for weak adhesion ($\gamma_W = 1000$)

contact forces and surface deformations at the contact boundary, which are not present for weak adhesion. The coloring shown in both figures visualizes the stress field σ_r, which is the stress in the radial direction from the indenter tip. For $\gamma_W = 2.17$, the range of σ_r lies between $-0.55\,E$ (blue: compression) and $0.09\,E$ (red: tension). Since the tensile stress region is localized in a narrow band at the contact boundary, a high mesh refinement is needed to capture these forces accurately. The adhesion forces lead to the reduction of the resultant contact force: For $\gamma_W = 1000$ we have $P = 0.549\,ER_0^2$, whereas for $\gamma_W = 2.17$ we only have $P = 0.506\,ER_0^2$.

7 CONCLUSION

The present paper introduces the coarse-grained contact model, a computational nanoscale contact model based on nonlinear continuum mechanics, and applies it to rubber adhesion. The model is validated against the analytical contact model of (Maugis 1992), which is based on the JKR model. The comparison shows an

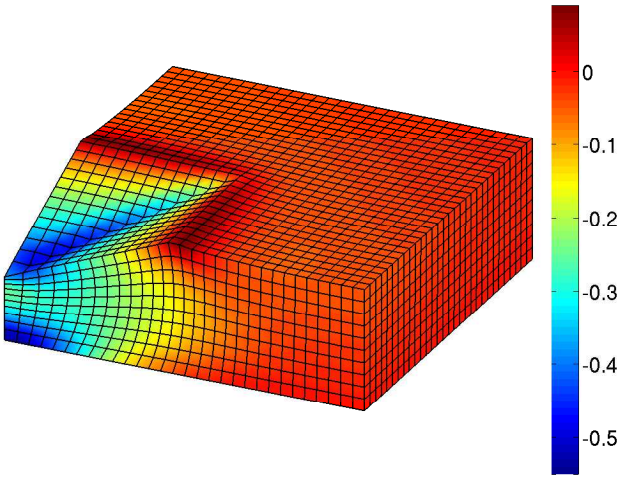

Figure 6: Nanoindentation of a rubber film: deformation and stress field under the indenter for strong adhesion ($\gamma_W = 2.17$)

excellent agreement between the models in the range where the JKR theory is applicable. Finally the computational contact model is applied to the analysis of the nanoindentation of a thin rubber film. The different behavior between weak and strong adhesion is illustrated and it is shown that strong adhesion computations require a much larger mesh refinement.

Further validation of the CGC model has been reported in our previous studies: In (Sauer and Li 2007b) the deformation of carbon-nanotubes is computed and compared to related studies in the literature. In (Sauer 2009) a multiscale contact model descibing the gecko adhesion mechanism is presented and it is shown than the computed pull-off forces of a single gecko spatula is in agreement to experimental data. A rigorous numerical analysis of the CGC model as well as details on the 3D finite element equations are discussed in (Sauer and Wriggers 2009).

The continuum mechanical framework gives the CGC model great flexibility and allows the accurate computation of a large class of contact interaction problems at the nanoscale. The CGC model can be applied for length scales down to a few nanometers before the continuum assumption breaks down. At this range the model is still far more efficient than molecular mechanics computations (Sauer and Li 2008).

REFERENCES

Israelachvili, J. N. (1991). *Intermolecular and Surface Forces* (2nd ed.). Academic Press.

Johnson, K. L., K. Kendall, and A. D. Roberts (1971). Surface energy and the contact of elastic solids. *Proc. R. Soc. Lond. A* **324**, 301–313.

Maugis, D. (1992). Adhesion of spheres: The jkr-dmt transition using a dugdale model. *L. Colloid Interface Sci.* **150**(1), 243–269.

Sauer, R. A. (2009). Multiscale modeling and simulation of the deformation and adhesion of a single gecko seta. *Comp. Meth. Biomech. Biomed. Engng.* **12**(6), 627–640.

Sauer, R. A. and S. Li (2007a). An atomic interaction-based continuum model for adhesive contact mechanics. *Finite Elem. Anal. Des.* **43**(5), 384–396.

Sauer, R. A. and S. Li (2007b). A contact mechanics model for quasi-continua. *Int. J. Numer. Meth. Engrg.* **71**(8), 931–962.

Sauer, R. A. and S. Li (2008). An atomistically enriched continuum model for nanoscale contact mechanics and its application to contact scaling. *J. Nanosci. Nanotech.* **8**(7), 3757–3773.

Sauer, R. A. and P. Wriggers (2009). Formulation and analysis of a 3D finite element implementation for adhesive contact at the nanoscale. *Comput. Methods Appl. Mech. Engrg.* **198**, 3871–3883.

Wriggers, P. (2008). *Nonlinear Finite Element Methods*. Springer.